Journal of

Applied and Computational Mechanics

Shahid Chamran
University of Ahvaz

Research Paper

Dynamics of Damped and Undamped Wave Natures of the Fractional Kraenkel-Manna-Merle System in Ferromagnetic Materials

Md. Nur Alam[1] , Md. Abdur Rahim[2] , Md. Najmul Hossain[3] , Cemil Tunç[4]

[1] Department of Mathematics, Pabna University of Science and Technology, Pabna, 6600, Bangladesh, Email: nuralam.pstu23@gmail.com; nuralam23@pust.ac.bd

[2] Department of Computer Science and Engineering, Pabna University of Science and Technology, Pabna, 6600, Bangladesh, Email: rahim_bds@yahoo.com

[3] Department of Electrical, Electronic and Communication Engineering, Pabna University of Science and Technology, Pabna, 6600, Bangladesh, Email: najmul_eece@pust.ac.bd

[4] Department of Mathematics, Faculty of Sciences, Van Yuzuncu Yil University, 65080, Van, Turkey, E-mail: cemtunc@yahoo.com

Abstract. This research considers the Kraenkel-Manna-Merle system with an M-truncated derivative (K-M-M-S-M-T-D) that defines the magnetic field propagation (M-F-P) in ferromagnetic materials with zero conductivity (F-M-Z-C) and uses the Sardar sub-equation method (S-S-E-M). Our goal is to acquire soliton solutions (SSs) of K-M-M-S-M-T-D via the S-S-E-M. To our knowledge, no one has considered the SSs to the K-M-M-S-MTD with or without a damping effect (DE) via the S-S-E-M. The SSs are achieved as the M-shape, periodic wave shape, W-shape, kink, anti-parabolic, and singular kink solitons in terms of free parameters. We utilize Maple to expose pictures in three-dimensional (3-D), contour and two-dimensional (2-D) for different values of fractional order (FO) of the got SSs, and we discuss the effect of the FO of the K-M-M-S-MTD via the S-S-E-M, which has not been discussed in the previous literature. All wave phenomena are applied to optical fiber communication, signal transmission, porous mediums, magneto-acoustic waves in plasma, electromagnetism, fluid dynamics, chaotic systems, coastal engineering, and so on. The achieved SSs prove that the S-S-E-M is very simple and effective for nonlinear science and engineering for examining nonlinear fractional differential equations (N-L-F-D-Es).

Keywords: The fractional Kraenkel-Manna-Merle system, M-Truncated derivative, Sardar sub-equation method, soliton solutions, nonlinear fractional differential equations.

1. Introduction

FMs have turned out to be a growing problem among investigators because of their numerous services in more than a few domains of NLSE including experimentation, magnetic motions, speed, nano-scale materials, network connectivity, massive data storage in numerous formats, power, and many more. The NLFDEs are operated in countless domains inclusive of optical fiber communication, mathematical biology, signal transmission, physics, porous mediums, quantum field theory, magneto-acoustic waves in plasma, neural physics, electromagnetism, solid state physics, fluid dynamics, chaotic systems, coastal engineering and many more [1-4]. Additionally, the concept of the M-T-D has been employed to illustrate a wide-ranging diversity of occurrences in numerous topics, for example, optical fiber communication, signal transmission, porous mediums, magneto-acoustic waves in plasma, electromagnetism, fluid dynamics, chaotic systems, coastal engineering, and so on. Because of the marvelous improvements in digital science to come face to face with the necessity for immense data and maximized storage, there has been a wealth of fascinating investigations on FMs. Consequently, tiny FM particles might currently be fabricated. FM is significant to get a higher quality sympathetic of the aspects of super- and micro-microstructures in nano-scale ferrous metals [5-7]. In the case of such tiny nano-particles, magnetization can be supposed of as homogeneous over these FPs and could be denoted by a magnetic moment. The magnetic moments in the dipolar motions permit FPs to exchange. Solitons are without interruption created as an outcome of these collaborations. Accordingly, a wide-ranging diversity of SS waves broadcasting occurrences has been scrutinized. The SS to the NLFDEs necessary to be attained with the intention of define whether the soliton is demolished after the collision. Though, determining NLFDEs has extended been a tough but essential endeavor. Thus, countless talented experts in the domains of NLSE have established a number of robust schemes for getting SSs, for example, the generalized projective Riccati equations technique [8], Sardar sub-equation scheme [9, 10], the fractional evolution process [11], the general algebraic scheme [12], the unified method [13, 14], the improved Kudryashov technique [15, 16], adapted (G'/G)-development scheme [17-23] and so many.

Consider the K-M-M-S-M-T-D:

$$\begin{cases} D_{i,t}^{\alpha;\beta}\dfrac{\partial V}{\partial x} - (V-k)\dfrac{\partial U}{\partial x} = 0, \\ D_{i,t}^{\alpha;\beta}\dfrac{\partial U}{\partial x} - V\dfrac{\partial V}{\partial x} = 0, \end{cases} \qquad (1)$$

where x and t are spatial and temporal variables, $U = U(x,t)$ is the external magnetic fields, $V = V(x,t)$ is the magnetization and k indicates the DE constraint that assistances to illuminate the concert of the magnetic materials, respectively. The fractional Kraenkel-Manna-Merle (KMM) model is actually associated more with physics and materials science rather than being specifically confined to mechanical engineering. It is a mathematical framework used to describe the dynamics of physical systems, particularly those exhibiting anomalous diffusion or fractional behavior, such as certain types of materials showing non-integer order dynamics. However, its application can extend to mechanical engineering, especially when dealing with materials exhibiting complex behaviors like ferromagnetic materials. Understanding the fractional KMM system in these materials can aid in designing mechanical components or systems where magnetic properties and material behavior play crucial roles. Therefore, while the KMM model itself might be more rooted in physics, its implications can definitely cross over into mechanical engineering practices.

Nguepjouo et al. [24] studied Eq. (1) and modified the following structure as:

$$\begin{cases} \dfrac{\partial^2 V}{\partial x \partial t} - (V-k)\dfrac{\partial U}{\partial x} = 0, \\ \dfrac{\partial^2 U}{\partial x \partial t} - V\dfrac{\partial V}{\partial x} = 0, \end{cases} \qquad (2)$$

which illuminates nonlinear tiny wave dissemination with F-M-Z-C in an external field. When $k = 0$ into Eq. (2), then Eq. (2) is integrable and lax pairings. Abundant experts have established countless schemes for getting the SSs to the K-M-M-S-M-T-D with $k = 0$, for example, the F-expansion technique [25], the simplified (G'/G)-development scheme [26], the truncated Painlevé scheme [27], the new sub-equation (NSE) method [28], the semi-inverse technique [29], Lie symmetry analysis method [30], Hirota's bilinear method [31], Darboux transformation [32], scattering inversion scheme [33], the multi-scale development scheme [34], the consistent tanh expansion scheme [35], Riccati model scheme [36], the mapping scheme [37], the auxiliary equation method [38], and so many. Still, the FD of the K-M-M-S-M-T-D via the SSEM has not been handled up until the present time.

The manuscript aims to employ the SSEM [9, 10] on the K-M-M-S-M-T-D system, exploring various soliton solutions such as the M-shape, dark soliton, periodic wave, double periodic shape, W-shape, kink, anti-parabolic, singular kink solitons, w-shape, and rogue wave profiles. By delving into previous literature discussions, it becomes apparent that certain wave profiles within the K-M-M-S-M-T-D system represent new findings. This research holds the potential to simulate extended wavelength water rollers through the incorporation of gently nonlinear restorative forces and regularity distribution. Furthermore, it presents applicability in modeling waves across diverse fields such as optical fiber communication, signal transmission, porous mediums, magneto-acoustic waves in plasma, electromagnetism, fluid dynamics, chaotic systems, and coastal engineering.

The novelty of the manuscript is to attain the SSs to the K-M-M-S-M-T-D in the with/without of a DE via the SSEM. We expand a few previous outcomes including the outcomes described in [25, 29]. The SSs obtainable at this time could be extremely cooperative to scientists in sympathetic significant nonlinear occurrences, since the KMMS-MTD demonstrates how nonlinear tiny wave dissemination with F-M-Z-C in an external field. Furthermore, we provide some graphical pictures produced via Maple software to examine the outcome of the FO on the got SSs to the K-M-M-S-M-T-D. The SSs are achieved as the M-shape, periodic wave shape, W-shape, kink, anti-parabolic, and singular kink solitons in terms of free parameters. All wave phenomena are applied to optical fiber communication, signal transmission, porous mediums, magneto-acoustic waves in plasma, electromagnetism, fluid dynamics, chaotic systems, coastal engineering, and so on. The acquired outcomes are helpful for the ultrashort light heartbeats in optical filaments. Our review model has much significance in quantum optics and liquid mechanics for making sense of the optical qualities of the femtosecond lasers and femtochemistry objects. Optical soliton annoyance is the foundation of the broadcast communications industry. This industry stays in business due to the wonder of soliton transmission innovation.

The manuscript's innovation lies in obtaining SSs for the K-M-M-S-M-T-D system, both with and without a differential equation, using the SSEM. We build upon prior findings, including those detailed in [25, 29]. The derived SSs offer valuable insights for scientists seeking a deeper understanding of significant nonlinear phenomena. The K-M-M-S-M-T-D model serves as a comprehensive framework illustrating nonlinear wave propagation, encompassing F-M-Z-C interactions within an external field. Additionally, we present graphical representations generated through Maple software, examining how changes in the FO impact the obtained SSs in the K-M-M-S-M-T-D system. These steady states manifest as various wave profiles, such as the M-shape, periodic wave shape, W-shape, kink, anti-parabolic, and singular kink solitons, characterized by their dependence on free parameters. Moreover, these wave phenomena find applications across diverse fields, including optical fiber communication, signal transmission, porous mediums, magneto-acoustic waves in plasma, electromagnetism, fluid dynamics, chaotic systems, coastal engineering, among others. The acquired outcomes hold particular significance in the realm of ultrashort light pulses within optical fibers. Our model contributes significantly to quantum optics and fluid mechanics, providing insights into the optical properties of femtosecond lasers and femtochemistry phenomena. The study of optical soliton propagation is fundamental to the telecommunications industry, as soliton transmission technology remains crucial for its operations and advancements. This technology forms the backbone of modern telecommunications, relying on the principles of optical soliton propagation for efficient data transmission and communication.

This article is structured into several sections for clarity and coherence. The initial section (Section 1) provides a comprehensive review of the literature, outlines the objectives, and offers background information. Section 2 elaborates on the M-Truncated derivative and introduces the traveling wave hypothesis. The subsequent section, Section 3, applies the proposed methodology to the K-M-M-S-M-T-D system. Moving forward, Section 4 delves into the presentation and discussion of the obtained results. Finally, Section 5 encapsulates the conclusions drawn from the study's findings and discussions.

2. M-T-D and Traveling Wave Hypothesis
2.1. M-T-D

Consider the function $f:[0,\infty) \to \Re$, $t > 0$, $0 < \alpha \le 1$, then definition of the local M-T-D of order $\alpha [D_{i,t}^{\alpha;\beta}]$ as follows:

$$D_{i,t}^{\alpha;\beta}\{f(t)\} = \lim_{\varepsilon \to 0} \frac{f(tE_{i,\beta}(\varepsilon t^{-\alpha})) - f(t)}{\varepsilon}, \quad \forall t > 0, \tag{3}$$

where $E_{i,\beta} = \sum_{k=0}^{i} \frac{W^k}{\Gamma(\beta k + 1)}$, for $\beta > 0$ and $W \in C$.

Sousa and Oliveira [39] provide a following theorem such that if V and U are differentiable functions and S_1, S_2 and S_3 are constants, then:

i. $D_{i,t}^{\alpha;\beta}(W_1 V + W_2 U) = W_1 D_{i,t}^{\alpha;\beta}(V) + W_2 D_{i,t}^{\alpha;\beta}(U)$;

ii. $D_{i,t}^{\alpha;\beta}(t^{W_3}) = \frac{W_3}{\Gamma(\beta + 1)} t^{W_3 - \alpha}$;

iii. $D_{i,t}^{\alpha;\beta}(VU) = V D_{i,t}^{\alpha;\beta}(U) + U D_{i,t}^{\alpha;\beta}(V)$;

iv. $D_{i,t}^{\alpha;\beta}(V)(t) = \frac{t^{1-\alpha}}{\Gamma(\beta + 1)} \frac{dV}{dt}$;

v. $D_{i,t}^{\alpha;\beta}(V \circ U)(t) = V'(U(t)) D_{i,t}^{\alpha;\beta} U(t)$.

2.2. Traveling wave hypothesis

Consider the complex transformation:

$$U(x,t) = U(\eta), \quad V(x,t) = V(\eta), \quad \eta = \eta_1 x + \frac{\eta_2 \Gamma(\beta + 1)}{\alpha} t^{\alpha}, \tag{4}$$

where $U(\eta)$ and $V(\eta)$ are the real functions, η_1 and η_2 are constants. Inserting Eq. (4) into Eq. (1), we obtain:

$$\begin{cases} \eta_1 \eta_2 U'' + k\eta_1 U' - \eta_1 UV' = 0, \\ \eta_1 \eta_2 V'' - \eta_1 VV' = 0. \end{cases} \tag{5}$$

Therefore, Eq. (5) becomes:

$$\begin{cases} \eta_2 U'' + kU' - UV' = 0, \\ \eta_2 V'' - VV' = 0. \end{cases} \tag{6}$$

Integrating the second equation in Eq. (6) once, we have:

$$V' = \frac{1}{2\eta_2} U^2 + \frac{r_0}{\eta_2}. \tag{7}$$

Substituting Eq. (7) into first equation in Eq. (6), we obtain:

$$U'' + S_3 U^3 + S_2 U^2 + S_1 U + S_0 = 0, \tag{8}$$

where $S_0 = \frac{kr_0}{\eta_2^2}$, $S_1 = \frac{-r_0}{\eta_2^2}$, $S_2 = \frac{k}{2\eta_2^2}$, $S_3 = \frac{-1}{2\eta_2^2}$.

3. Analysis of Soliton Solutions

According to the SSEM, we have:

$$U = F_0 + F_1 \Phi^1. \tag{9}$$

From Eqs. (9) and (8), then we find:

Cluster-01:

$$k = \pm 3\eta_2 \sqrt{\frac{-\beta}{2}}, \quad r_0 = \frac{\beta \eta_2^2}{4}, \quad F_0 = \pm \eta_2 \sqrt{\frac{-\beta}{2}}, \quad F_1 = \pm 2\eta_2. \tag{10}$$

Cluster-02:

$$k = 0, \quad r_0 = \beta \eta_2^2, \quad F_0 = 0, \quad F_1 = \pm 2\eta_2. \tag{11}$$

3.1. The K-M-M-S-M-T-D with the damping term

Substituting the above values in Cluster-01 into Eq. (9), then we achieve:

Group-01: If $a = 0$ and $b > 0$, then:

$$U_1^{\pm}(\eta) = \pm i\eta_2 \sqrt{\frac{\beta}{2}} \pm 2\eta_2 \{\pm i\sqrt{\lambda\mu b} \times \frac{2}{\lambda e^{\sqrt{b}\eta} + \mu e^{-\sqrt{b}\eta}}\}, \tag{12}$$

$$U_2^{\pm}(\eta) = \pm i\eta_2\sqrt{\frac{\beta}{2}} \pm 2\eta_2\{\pm i\sqrt{\lambda\mu b} \times \frac{2}{\lambda e^{\sqrt{b}\eta} - \mu e^{-\sqrt{b}\eta}}\}. \tag{13}$$

Group-02: If $a = 0$ and $b < 0$, then:

$$U_3^{\pm}(\eta) = \pm i\eta_2\sqrt{\frac{\beta}{2}} \pm 2\eta_2\{\pm i\sqrt{\lambda\mu b} \times \frac{2}{\lambda e^{-\sqrt{b}\eta} + \mu e^{\sqrt{b}\eta}}\}, \tag{14}$$

$$U_4^{\pm}(\eta) = \pm i\eta_2\sqrt{\frac{\beta}{2}} \pm 2\eta_2\{\pm i\sqrt{\lambda\mu b} \times \frac{2}{\lambda e^{-\sqrt{b}\eta} - \mu e^{\sqrt{b}\eta}}\}. \tag{15}$$

Group-03: If $a = \frac{b^2}{4}$ and $b < 0$, then:

$$U_5^{\pm}(\eta) = \pm i\eta_2\sqrt{\frac{\beta}{2}} \pm 2\eta_2\{\pm i\sqrt{\frac{b}{2}} \times \frac{\lambda e^{i\sqrt{\frac{b}{2}}\eta} - \mu e^{-i\sqrt{\frac{b}{2}}\eta}}{\lambda e^{i\sqrt{\frac{b}{2}}\eta} + \mu e^{-i\sqrt{\frac{b}{2}}\eta}}\}, \tag{16}$$

$$U_6^{\pm}(\eta) = \pm i\eta_2\sqrt{\frac{\beta}{2}} \pm 2\eta_2\{\pm i\sqrt{\frac{b}{2}} \times \frac{\lambda e^{i\sqrt{\frac{b}{2}}\eta} + \mu e^{-i\sqrt{\frac{b}{2}}\eta}}{\lambda e^{i\sqrt{\frac{b}{2}}\eta} - \mu e^{-i\sqrt{\frac{b}{2}}\eta}}\}, \tag{17}$$

$$U_7^{\pm}(\eta) = \pm i\eta_2\sqrt{\frac{\beta}{2}} \pm 2\eta_2\{\pm i\sqrt{\frac{b}{2}} \times \{\frac{\lambda e^{i\sqrt{2b}\eta} - \mu e^{-i\sqrt{2b}\eta}}{\lambda e^{i\sqrt{2b}\eta} + \mu e^{-i\sqrt{2b}\eta}} \pm i\sqrt{\lambda\mu} \times \frac{2}{\lambda e^{i\sqrt{2b}\eta} + \mu e^{-i\sqrt{2b}\eta}}\}\}, \tag{18}$$

$$U_8^{\pm}(\eta) = \pm i\eta_2\sqrt{\frac{\beta}{2}} \pm 2\eta_2\{\pm i\sqrt{\frac{b}{2}} \times \{\frac{\lambda e^{i\sqrt{2b}\eta} + \mu e^{-i\sqrt{2b}\eta}}{\lambda e^{i\sqrt{2b}\eta} - \mu e^{-i\sqrt{2b}\eta}} \pm \sqrt{\lambda\mu} \times \frac{2}{\lambda e^{i\sqrt{2b}\eta} - \mu e^{-i\sqrt{2b}\eta}}\}\}, \tag{19}$$

$$U_9^{\pm}(\eta) = \pm i\eta_2\sqrt{\frac{\beta}{2}} \pm 2\eta_2\{\pm i\sqrt{\frac{b}{8}} \times \{\frac{\lambda e^{i\sqrt{\frac{b}{8}}\eta} - \mu e^{-i\sqrt{\frac{b}{8}}\eta}}{\lambda e^{i\sqrt{\frac{b}{8}}\eta} + \mu e^{-i\sqrt{\frac{b}{8}}\eta}} \pm \sqrt{\lambda\mu} \times \frac{\lambda e^{i\sqrt{\frac{b}{8}}\eta} + \mu e^{-i\sqrt{\frac{b}{8}}\eta}}{\lambda e^{i\sqrt{\frac{b}{8}}\eta} - \mu e^{-i\sqrt{\frac{b}{8}}\eta}}\}\}. \tag{20}$$

Group-04: If $a = \frac{b^2}{4}$ and $b > 0$, then:

$$U_{10}^{\pm}(\eta) = \pm i\eta_2\sqrt{\frac{\beta}{2}} \pm 2\eta_2\{\pm\sqrt{\frac{b}{2}} \times (-i\frac{\lambda e^{-\sqrt{\frac{b}{2}}\eta} - \mu e^{\sqrt{\frac{b}{2}}\eta}}{\lambda e^{-\sqrt{\frac{b}{2}}\eta} + \mu e^{\sqrt{\frac{b}{2}}\eta}})\}, \tag{21}$$

$$U_{11}^{\pm}(\eta) = \pm i\eta_2\sqrt{\frac{\beta}{2}} \pm 2\eta_2\{\pm\sqrt{\frac{b}{2}} \times (i\frac{\lambda e^{-\sqrt{\frac{b}{2}}\eta} + \mu e^{\sqrt{\frac{b}{2}}\eta}}{\lambda e^{-\sqrt{\frac{b}{2}}\eta} - \mu e^{\sqrt{\frac{b}{2}}\eta}})\}, \tag{22}$$

$$U_{12}^{\pm}(\eta) = \pm i\eta_2\sqrt{\frac{\beta}{2}} \pm 2\eta_2\{\pm\sqrt{\frac{b}{2}} \times \{-i\frac{\lambda e^{i\sqrt{2b}\eta} - \mu e^{-i\sqrt{2b}\eta}}{\lambda e^{i\sqrt{2b}\eta} + \mu e^{-i\sqrt{2b}\eta}} \pm i\sqrt{\lambda\mu} \times \frac{2}{\lambda e^{i\sqrt{2b}\eta} + \mu e^{-i\sqrt{2b}\eta}}\}\}, \tag{23}$$

$$U_{13}^{\pm}(\eta) = \pm i\eta_2\sqrt{\frac{\beta}{2}} \pm 2\eta_2\{\pm\sqrt{\frac{b}{2}} \times \{-i\frac{\lambda e^{i\sqrt{2b}\eta} + \mu e^{-i\sqrt{2b}\eta}}{\lambda e^{i\sqrt{2b}\eta} - \mu e^{-i\sqrt{2b}\eta}} \pm \sqrt{\lambda\mu} \times \frac{2}{\lambda e^{i\sqrt{2b}\eta} - \mu e^{-i\sqrt{2b}\eta}}\}\}, \tag{24}$$

$$U_{14}^{\pm}(\eta) = \pm i\eta_2\sqrt{\frac{\beta}{2}} \pm 2\eta_2\{\pm\sqrt{\frac{b}{8}} \times \{-i\frac{\lambda e^{i\sqrt{\frac{b}{8}}\eta} - \mu e^{-i\sqrt{\frac{b}{8}}\eta}}{\lambda e^{i\sqrt{\frac{b}{8}}\eta} + \mu e^{-i\sqrt{\frac{b}{8}}\eta}} \pm \sqrt{\lambda\mu} \times i\frac{\lambda e^{i\sqrt{\frac{b}{8}}\eta} + \mu e^{-i\sqrt{\frac{b}{8}}\eta}}{\lambda e^{i\sqrt{\frac{b}{8}}\eta} - \mu e^{-i\sqrt{\frac{b}{8}}\eta}}\}\}. \tag{25}$$

3.2. The K-M-M-S-M-T-D without the damping term

Substituting the values in Cluster-02 into Eq. (9), then we achieve:

Group-01: If $a = 0$ and $b > 0$, then:

$$U_{15}^{\pm}(\eta) = \pm 2\eta_2\{\pm i\sqrt{\lambda\mu b} \times \frac{2}{\lambda e^{\sqrt{b}\eta} + \mu e^{-\sqrt{b}\eta}}\}, \tag{26}$$

$$U_{16}^{\pm}(\eta) = \pm 2\eta_2 \{\pm i\sqrt{\lambda\mu b} \times \frac{2}{\lambda e^{\sqrt{b}\eta} - \mu e^{-\sqrt{b}\eta}}\}. \tag{27}$$

Group-02: If $a = 0$ and $b < 0$, then:

$$U_{17}^{\pm}(\eta) = \pm 2\eta_2 \{\pm i\sqrt{\lambda\mu b} \times \frac{2}{\lambda e^{-\sqrt{b}\eta} + \mu e^{\sqrt{b}\eta}}\}, \tag{28}$$

$$U_{18}^{\pm}(\eta) = \pm 2\eta_2 \{\pm i\sqrt{\lambda\mu b} \times \frac{2}{\lambda e^{-\sqrt{b}\eta} - \mu e^{\sqrt{b}\eta}}\}. \tag{29}$$

Group-03: If $a = \frac{b^2}{4}$ and $b < 0$, then:

$$U_{19}^{\pm}(\eta) = \pm 2\eta_2 \{\pm i\sqrt{\frac{b}{2}} \times \frac{\lambda e^{i\sqrt{\frac{b}{2}}\eta} - \mu e^{-i\sqrt{\frac{b}{2}}\eta}}{\lambda e^{i\sqrt{\frac{b}{2}}\eta} + \mu e^{-i\sqrt{\frac{b}{2}}\eta}}\}, \tag{30}$$

$$U_{20}^{\pm}(\eta) = \pm 2\eta_2 \{\pm i\sqrt{\frac{b}{2}} \times \frac{\lambda e^{i\sqrt{\frac{b}{2}}\eta} + \mu e^{-i\sqrt{\frac{b}{2}}\eta}}{\lambda e^{i\sqrt{\frac{b}{2}}\eta} - \mu e^{-i\sqrt{\frac{b}{2}}\eta}}\}, \tag{31}$$

$$U_{21}^{\pm}(\eta) = \pm 2\eta_2 \{\pm i\sqrt{\frac{b}{2}} \times \{\frac{\lambda e^{i\sqrt{2b}\eta} - \mu e^{-i\sqrt{2b}\eta}}{\lambda e^{i\sqrt{2b}\eta} + \mu e^{-i\sqrt{2b}\eta}} \pm i\sqrt{\lambda\mu} \times \frac{2}{\lambda e^{i\sqrt{2b}\eta} + \mu e^{-i\sqrt{2b}\eta}}\}\}, \tag{32}$$

$$U_{22}^{\pm}(\eta) = \pm 2\eta_2 \{\pm i\sqrt{\frac{b}{2}} \times \{\frac{\lambda e^{i\sqrt{2b}\eta} + \mu e^{-i\sqrt{2b}\eta}}{\lambda e^{i\sqrt{2b}\eta} - \mu e^{-i\sqrt{2b}\eta}} \pm \sqrt{\lambda\mu} \times \frac{2}{\lambda e^{i\sqrt{2b}\eta} - \mu e^{-i\sqrt{2b}\eta}}\}\}, \tag{33}$$

$$U_{23}^{\pm}(\eta) = \pm 2\eta_2 \{\pm i\sqrt{\frac{b}{8}} \times \{\frac{\lambda e^{i\sqrt{\frac{b}{8}}\eta} - \mu e^{-i\sqrt{\frac{b}{8}}\eta}}{\lambda e^{i\sqrt{\frac{b}{8}}\eta} + \mu e^{-i\sqrt{\frac{b}{8}}\eta}} \pm \sqrt{\lambda\mu} \times \frac{\lambda e^{i\sqrt{\frac{b}{8}}\eta} + \mu e^{-i\sqrt{\frac{b}{8}}\eta}}{\lambda e^{i\sqrt{\frac{b}{8}}\eta} - \mu e^{-i\sqrt{\frac{b}{8}}\eta}}\}\}. \tag{34}$$

Group-04: If $a = \frac{b^2}{4}$ and $b > 0$, then:

$$U_{24}^{\pm}(\eta) = \pm 2\eta_2 \{\pm \sqrt{\frac{b}{2}} \times (-i\frac{\lambda e^{-\sqrt{\frac{b}{2}}\eta} - \mu e^{\sqrt{\frac{b}{2}}\eta}}{\lambda e^{-\sqrt{\frac{b}{2}}\eta} + \mu e^{\sqrt{\frac{b}{2}}\eta}})\}, \tag{35}$$

$$U_{25}^{\pm}(\eta) = \pm 2\eta_2 \{\pm \sqrt{\frac{b}{2}} \times (i\frac{\lambda e^{-\sqrt{\frac{b}{2}}\eta} + \mu e^{\sqrt{\frac{b}{2}}\eta}}{\lambda e^{-\sqrt{\frac{b}{2}}\eta} - \mu e^{\sqrt{\frac{b}{2}}\eta}})\}, \tag{36}$$

$$U_{26}^{\pm}(\eta) = \pm 2\eta_2 \{\pm \sqrt{\frac{b}{2}} \times \{-i\frac{\lambda e^{i\sqrt{2b}\eta} - \mu e^{-i\sqrt{2b}\eta}}{\lambda e^{i\sqrt{2b}\eta} + \mu e^{-i\sqrt{2b}\eta}} \pm i\sqrt{\lambda\mu} \times \frac{2}{\lambda e^{i\sqrt{2b}\eta} + \mu e^{-i\sqrt{2b}\eta}}\}\}, \tag{37}$$

$$U_{27}^{\pm}(\eta) = \pm 2\eta_2 \{\pm \sqrt{\frac{b}{2}} \times \{-i\frac{\lambda e^{i\sqrt{2b}\eta} + \mu e^{-i\sqrt{2b}\eta}}{\lambda e^{i\sqrt{2b}\eta} - \mu e^{-i\sqrt{2b}\eta}} \pm \sqrt{\lambda\mu} \times \frac{2}{\lambda e^{i\sqrt{2b}\eta} - \mu e^{-i\sqrt{2b}\eta}}\}\}, \tag{38}$$

$$U_{28}^{\pm}(\eta) = \pm 2\eta_2 \{\pm \sqrt{\frac{b}{8}} \times \{-i\frac{\lambda e^{i\sqrt{\frac{b}{8}}\eta} - \mu e^{-i\sqrt{\frac{b}{8}}\eta}}{\lambda e^{i\sqrt{\frac{b}{8}}\eta} + \mu e^{-i\sqrt{\frac{b}{8}}\eta}} \pm \sqrt{\lambda\mu} \times i\frac{\lambda e^{i\sqrt{\frac{b}{8}}\eta} + \mu e^{-i\sqrt{\frac{b}{8}}\eta}}{\lambda e^{i\sqrt{\frac{b}{8}}\eta} - \mu e^{-i\sqrt{\frac{b}{8}}\eta}}\}\}. \tag{39}$$

4. Results and Discussion

In comparison to the research outlined in [25], our study represents a significant advancement in the exploration of the K-M-M-S-M-T-D. Alshammari et al. [25] dedicated their efforts to comprehensively investigating the K-M-M-S-M-T-D, meticulously deriving twenty-eight solutions primarily centered around trigonometric and hyperbolic functions. Similarly, our research mirrors their findings by also yielding a count of twenty-eight solutions. This outcome marks a pivotal achievement, as it signifies a substantial expansion in the range and diversity of solutions, encompassing not only trigonometric and hyperbolic functions but also extending to encompass rational, periodic, and hyperbolic forms. Moreover, our study delves deeper into the nuances of the K-

M-M-S-M-T-D by meticulously examining the influence of individual parameters, fractional elements, and nonlinearities characterized by general parametric powers on the obtained results. Our investigation also ventures into the effects arising from variations in the order of derivatives on the resultant wave profile. By delving into these intricacies, we sought a more profound comprehension of the nature and behavior exhibited by these solutions. Recognizing the complexity inherent in these findings, we acknowledge the importance of visual aids in elucidating the essence and dynamics of these solutions. Hence, graphical illustrations have been employed to offer a more intuitive and accessible understanding of the intricate relationships and patterns observed within the scope of our research. These visual representations serve as indispensable tools in comprehending the multifaceted nature of the solutions derived from the K-M-M-S-M-T-D, facilitating a more comprehensive grasp of their behavior and characteristics. In this domain, we have successfully derived twenty-eight SSs $U_1^{\pm}(\ell)$ $(1 \leq i \leq 28)$ for the K-M-M-S-M-T-D, both with and without the presence of a differential equation (DE). These SSs encompass a diverse range of wave solutions, including V-shaped periodic waves, solitary solitons, M-shaped periodic wave solutions, various forms of periodic waves, singular kink-type shapes, kink shapes, and numerous other types of steady states achieved through the use of the SSEM. Our investigation specifically focused on observing how the wave shapes of these steady states transformed under varying values of the FO. To gain a comprehensive understanding of the nature and behavior exhibited by these solutions, graphical representations play a pivotal role. Consequently, we have utilized a variety of graphical depictions, such as 3-D plots, contour plots, and 2D representations, to illustrate the waveforms corresponding to different values of the FO for the obtained SSs $U_1^{\pm}(\ell)$, $U_3^{\pm}(\ell)$, $U_5^{\pm}(\ell)$, $U_{10}^{\pm}(\eta)$, $U_{14}^{\pm}(\eta)$, $U_{15}^{\pm}(\eta)$, $U_{17}^{\pm}(\eta)$, $U_{19}^{\pm}(\eta)$, $U_{23}^{\pm}(\eta)$ and $U_{26}^{\pm}(\eta)$. Figures 1 through 10 showcases these graphical depictions, offering a visual insight into the diverse range of SSs derived in our study. These visual representations serve as indispensable tools in comprehending the complex dynamics and characteristics inherent in the solutions of the K-M-M-S-M-T-D, facilitating a more intuitive understanding of their behavior and variations.

Different behaviors associated with specific values of independent parameters are visually depicted through 3-D, 2-D, and contour plots. In Fig. 1, a variety of wave behaviors are showcased, exhibiting distinct characteristics. The portrayal includes bright-dark wave phenomena of $U_1^{\pm}(\ell)$ for $\alpha = 0.20$, $\beta = 0.10$, $\mu = 0.50$, $\lambda = 0.20$, $\alpha = 0.20$, $\eta_1 = \eta_2 = 1$. The figures consist of 3-D representations (both real and complex) denoted as (a) and (b), respectively, along with corresponding contour plots represented as (c) and (d). Within Fig. 1(a), 1(b), 1(c), and 1(d), the alterations in α, demonstrating the effects of spatial fractionation, are presented. Specifically, the influence of α variations on the wave behaviors is depicted in Fig. 1(e) and 1(f), providing a nuanced understanding of how changes in this parameter affect the observed wave patterns. Figure 2 showcases periodic wave patterns of $U_3^{\pm}(\ell)$ corresponding to $\alpha = 0.10$, $\beta = 0.10$, $\mu = 10$, $\lambda = 20$, $\eta_1 = 0.10$, $\eta_2 = 0.20$. This figure includes 3-D representations denoted as (a) and (b) for real and complex domains, respectively, alongside contour plots represented as (c) and (d). These graphical depictions within Fig. 2(a), 2(b), 2(c), and 2(d) illustrate the distinct characteristics of periodic wave behavior. Additionally, the impact of spatial fractionation, resulting from alterations in the α parameter, is highlighted in Fig. 2(e) and 2(f). These illustrations serve to demonstrate how changes in α affect the spatial properties and features of the observed periodic wave patterns.

Figure 3 portrays singular periodic wave patterns of $U_5^{\pm}(\ell)$ corresponding to $\alpha = 0.30$, $\beta = 0.25$, $\mu = 10$, $\lambda = 20$, $\eta_1 = 0.30$, $\eta_2 = 0.40$. This illustration encompasses 3-D representations denoted as (a) and (b) for the real and complex domains, respectively. Additionally, contour plots represented as (c) and (d) are featured within Fig. 3(a), 3(b), 3(c), and 3(d), offering insights into the distinct characteristics of singular periodic wave behavior. Furthermore, the impact of spatial fractionation resulting from variations in the α parameter is elucidated in Fig. 3(e) and 3(f). These depictions serve to highlight how changes in α influence the spatial properties and features exhibited by the singular periodic wave patterns.
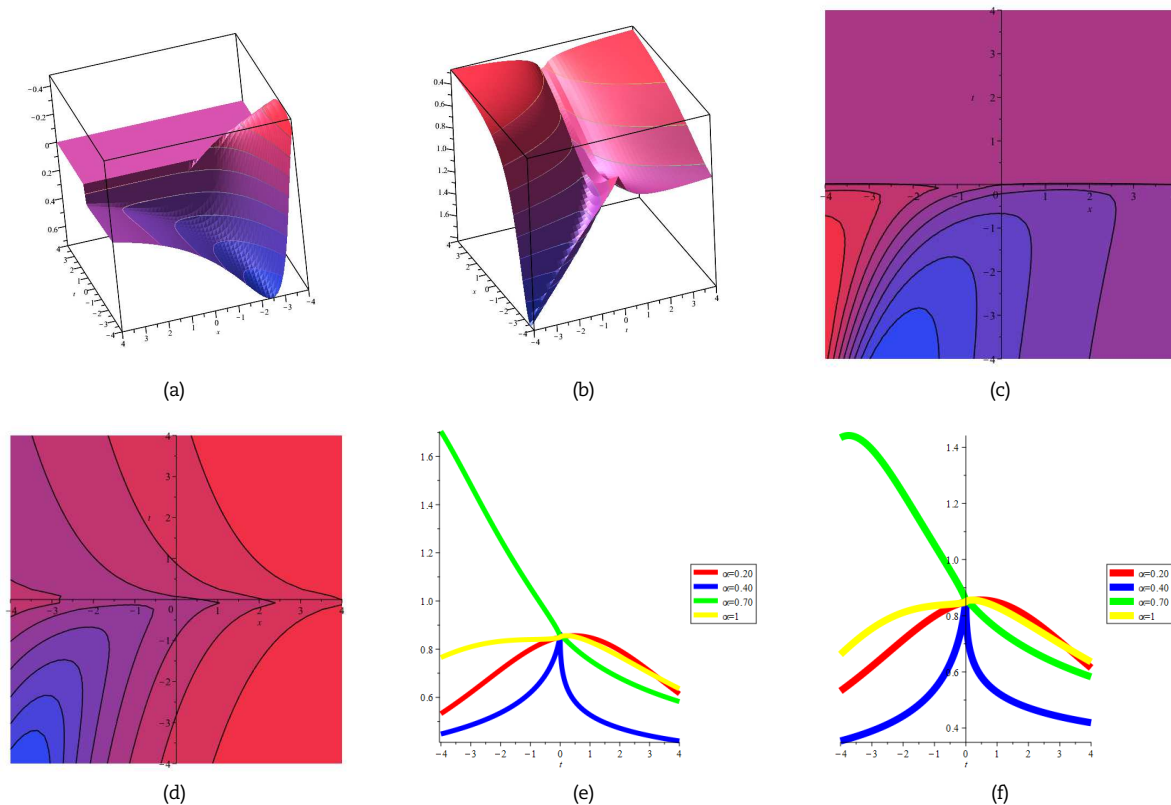

| (a) | (b) | (c) |
| (d) | (e) | (f) |

Fig. 1. 3-D [(a) real and (b) complex], Contour [(c) real and (d) complex], and 2-D graph [(e) real and (f) complex] picture of $U_1^{\pm}(\eta)$ for $\alpha = 0.20$, $\beta = 0.10$, $\mu = 0.50$, $\lambda = 0.20$, $\alpha = 0.20$, $\eta_1 = \eta_2 = 1$.
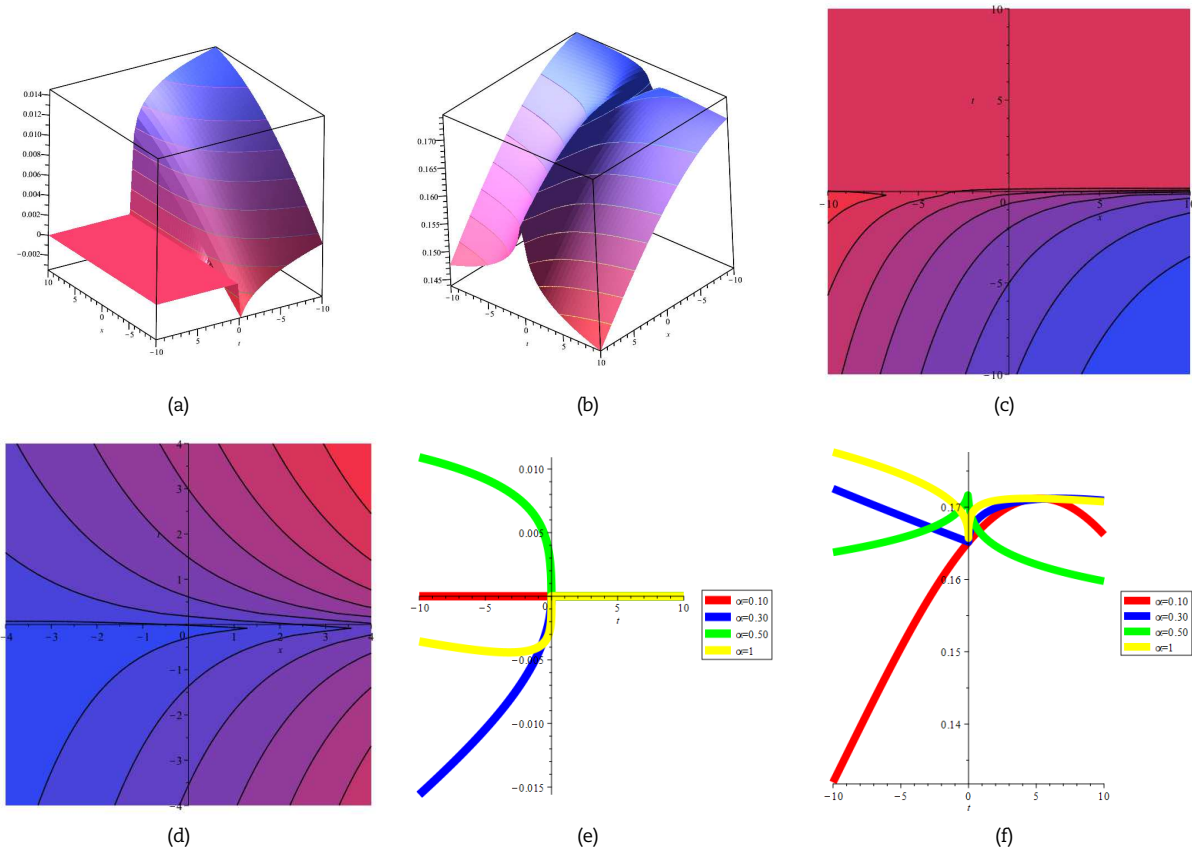
Fig. 2. 3-D [(a) real and (b) complex], Contour [(c) real and (d) complex], and 2-D graph [(e) real and (f) complex] picture of $U_3^{\pm}(\eta)$ for $\alpha = 0.10$, $\beta = 0.10$, $\mu = 10$, $\lambda = 20$, $\eta_1 = 0.10$, $\eta_2 = 0.20$.
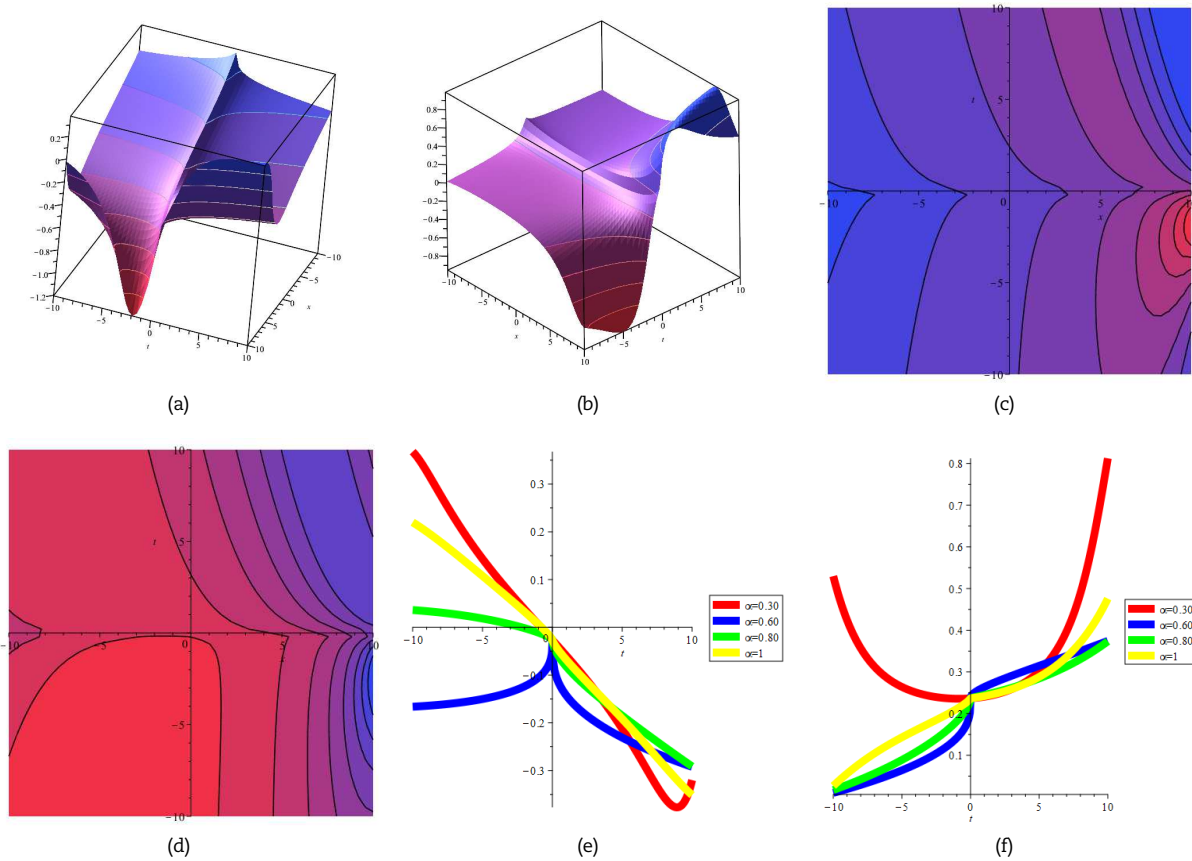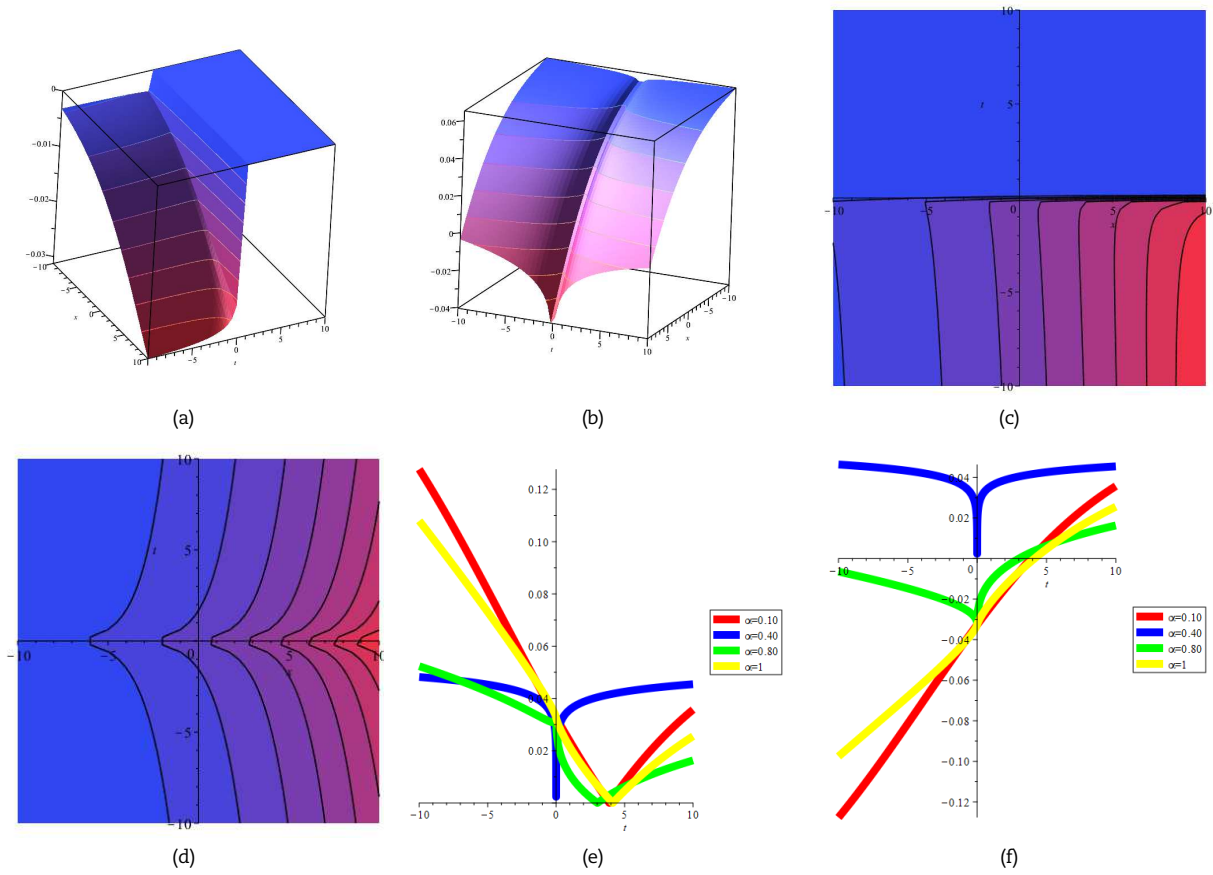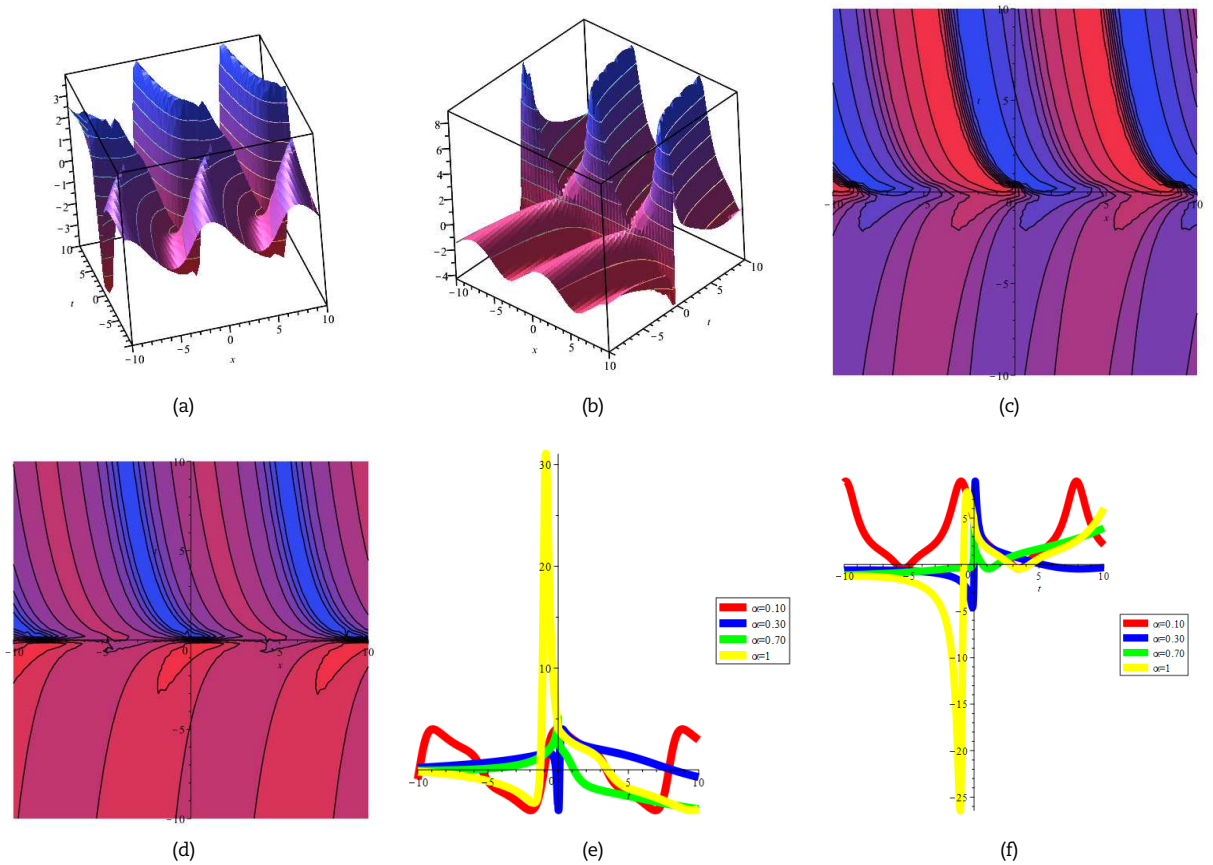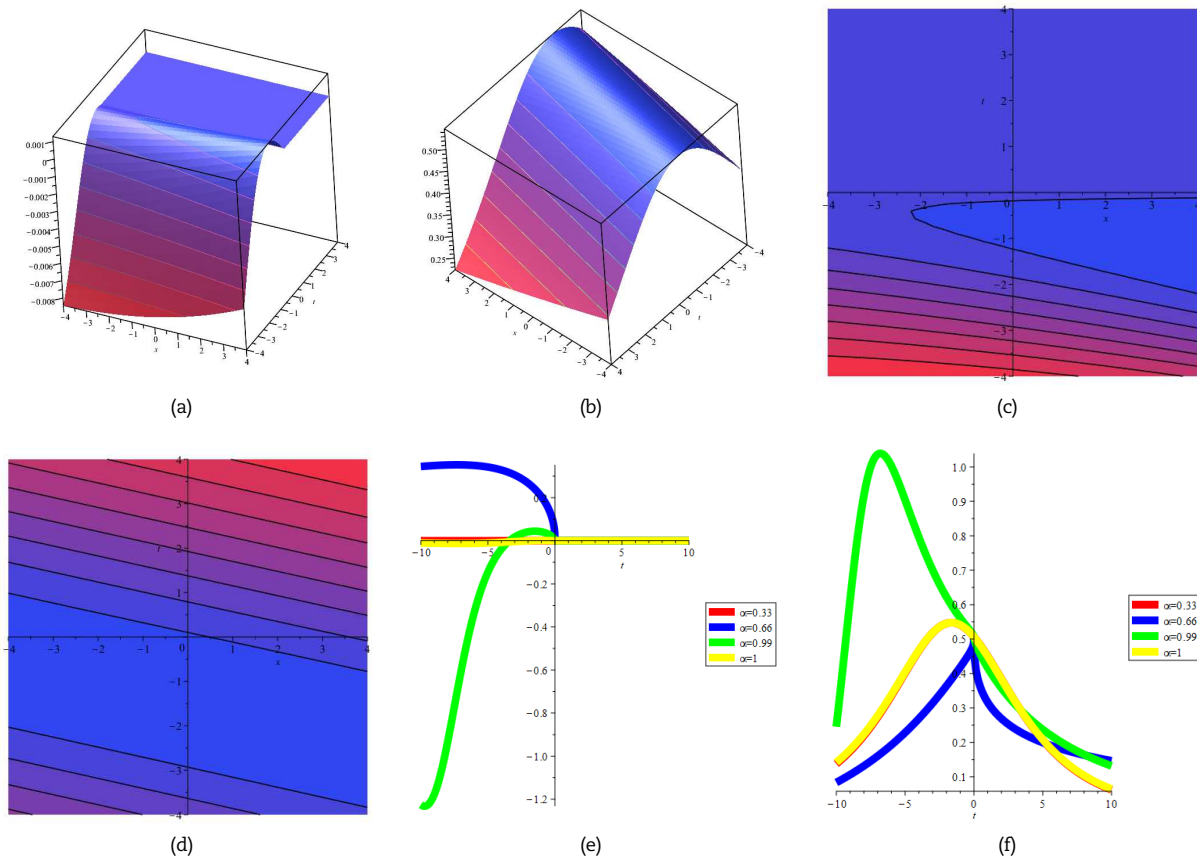

Fig. 3. 3-D [(a) real and (b) complex], Contour [(c) real and (d) complex], and 2-D graph [(e) real and (f) complex] picture of $U_5^{\pm}(\eta)$ for $\alpha = 0.30$, $\beta = 0.25$, $\mu = 10$, $\lambda = 20$, $\eta_1 = 0.30$, $\eta_2 = 0.40$.

Fig. 4. 3-D [(a) real and (b) complex], Contour [(c) real and (d) complex], and 2-D graph [(e) real and (f) complex] picture of $U_{10}^{\pm}(\eta)$ for $\alpha = 0.10$, $\beta = 0.01$, $\mu = 1$, $\lambda = 2$, $\eta_1 = 1$, $\eta_2 = -1$.

Fig. 5. 3-D [(a) real and (b) complex], Contour [(c) real and (d) complex], and 2-D graph [(e) real and (f) complex] picture of $U_{14}^{\pm}(\eta)$ for $\alpha = 0.10$, $\beta = 1$, $\mu = 1$, $\lambda = 2$, $\eta_1 = 1$, $\eta_2 = 1$.

Fig. 6. 3-D [(a) real and (b) complex], Contour [(c) real and (d) complex], and 2-D graph [(e) real and (f) complex] picture of $U_{15}{}^{\pm}(\eta)$ for $\alpha = 0.99$, $\beta = 0.30$, $\mu = 1$, $\lambda = 2$, $\eta_1 = 0.10$, $\eta_2 = 0.50$.
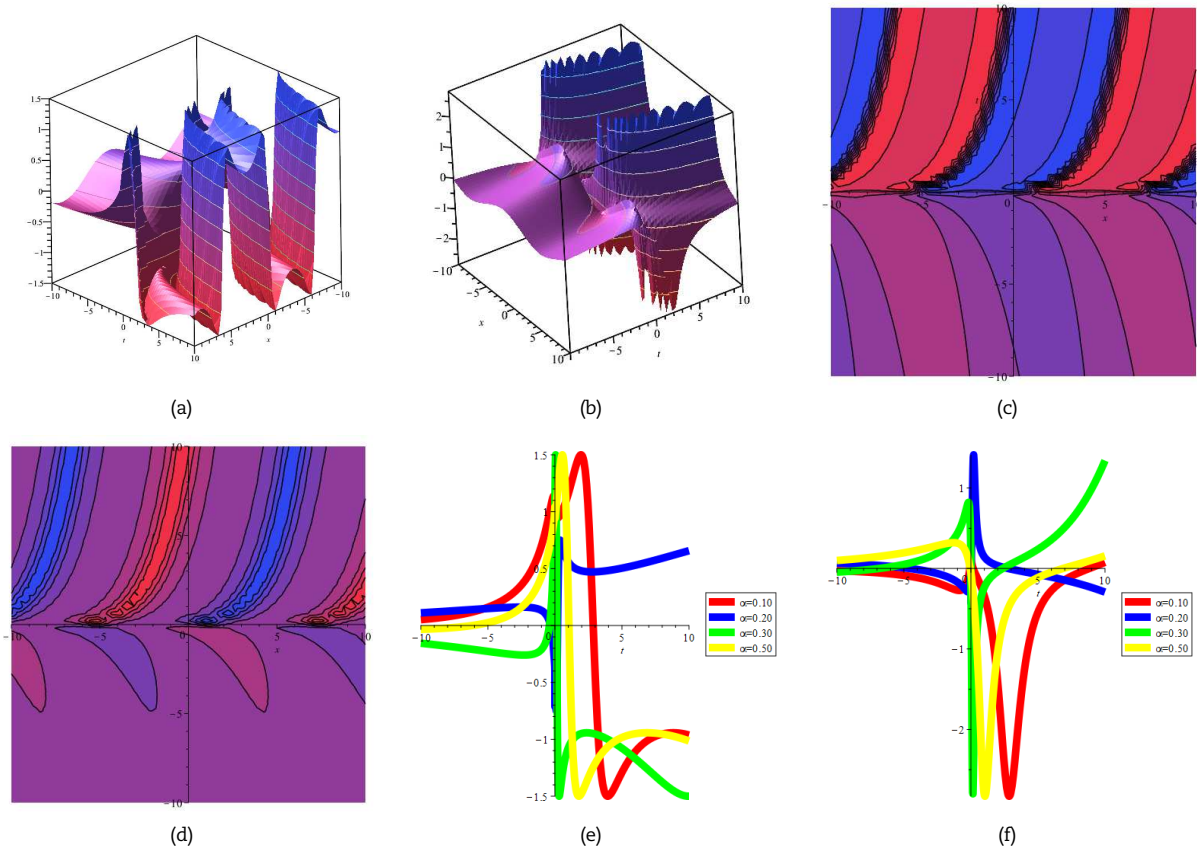

Fig. 7. 3-D [(a) real and (b) complex], Contour [(c) real and (d) complex], and 2-D graph [(e) real and (f) complex] picture of $U_{17}{}^{\pm}(\eta)$ for $\alpha = 0.10$, $\beta = -0.25$, $\mu = 1$, $\lambda = 2$, $\eta_1 = -1$, $\eta_2 = 1$.

Figure 4 exhibits multiple periodic wave patterns of $U_{10}^{\pm}(\eta)$ corresponding to $\alpha = 0.10$, $\beta = 0.01$, $\mu = 1$, $\lambda = 2$, $\eta_1 = 1$, $\eta_2 = -1$. This presentation encompasses 3-D representations denoted as (a) and (b) for the real and complex domains, respectively. Additionally, contour plots represented as (c) and (d) are depicted within Fig. 4(a), 4(b), 4(c), and 4(d), offering insights into the diverse characteristics of multiple periodic wave behavior. Moreover, Fig. 4(e) and 4(f) illustrate the influence of spatial fractionation resulting from variations in the α parameter. These representations elucidate how changes in α impact the spatial attributes and features exhibited by the multiple periodic wave patterns.

Figure 5 displays multiple bright-dark periodic wave patterns of $U_{14}^{\pm}(\eta)$ corresponding to $\alpha = 0.10$, $\beta = 1$, $\mu = 1$, $\lambda = 2$, $\eta_1 = 1$, $\eta_2 = 1$. This graphical representation comprises 3-D depictions denoted as (a) and (b) for the real and complex domains, respectively. Additionally, contour plots represented as (c) and (d) are presented within Fig. 5(a), 5(b), 5(c), and 5(d), elucidating the distinctive characteristics of multiple bright-dark periodic wave behavior. Furthermore, Fig. 5(e) and 5(f) delineate the impact of spatial fractionation resulting from variations in the α parameter. These illustrations provide insights into how alterations in α influence the spatial properties and features exhibited by the multiple bright-dark periodic wave patterns.

Figure 6 exhibits multiple bright-dark periodic wave patterns of $U_{15}^{\pm}(\eta)$ corresponding to $\alpha = 0.99$, $\beta = 0.30$, $\mu = 1$, $\lambda = 2$, $\eta_1 = 0.10$, $\eta_2 = 0.50$. This visual representation comprises 3-D depictions labeled as (a) and (b) for the real and complex domains, respectively. Additionally, contour plots represented as (c) and (d) are presented within Fig. 6(a), 6(b), 6(c), and 6(d), delineating the unique characteristics of multiple bright-dark periodic wave behavior. Moreover, Fig. 6(e) and 6(f) illustrate the repercussions of spatial fractionation resulting from variations in the α parameter. These visual depictions elucidate how changes in α influence the spatial attributes and features manifested by the multiple bright-dark periodic wave patterns.

In Fig. 7: M-shape periodic wave $U_{17}^{\pm}(\eta)$ for $\alpha = 0.10$, $\beta = -0.25$, $\mu = 1$, $\lambda = 2$, $\eta_1 = -1$, $\eta_2 = 1$, 3-D [(a) real and (b) complex], Contour [(c) real and (d) complex], in Fig. 7(a), 7(b), 7(c) and 7(d); effects of space fractionally due to changes of α are presented in Fig. 7(e) and 7(f). In Fig. 8: rogue wave $U_{19}^{\pm}(\eta)$ for $\alpha = 0.50$, $\beta = 0.25$, $\mu = 1$, $\lambda = 2$, $\eta_1 = 1$, $\eta_2 = 1$, 3-D [(a) real and (b) complex], Contour [(c) real and (d) complex], in Fig. 8(a), 8(b), 8(c) and 8(d); effects of space fractionally due to changes of α are presented in Fig. 8(e) and 8(f). In Fig. 9: singular periodic wave $U_{23}^{\pm}(\eta)$ for $\alpha = 0.50$, $\beta = 0.25$, $\mu = 1$, $\lambda = 2$, $\eta_1 = 1$, $\eta_2 = 1$, 3-D [(a) real and (b) complex], Contour [(c) real and (d) complex], in Fig. 9(a), 9(b), 9(c) and 9(d); effects of space fractionally due to changes of α are presented in Fig. 9(e) and 9(f). In Fig. 10: M-shape wave $U_{26}^{\pm}(\eta)$ for $\alpha = 0.25$, $\beta = 0.10$, $\mu = 1$, $\lambda = 2$, $\eta_1 = 1$, $\eta_2 = 1$, 3-D [(a) real and (b) complex], Contour [(c) real and (d) complex], in Fig. 10(a), 10(b), 10(c) and 10(d); effects of space fractionally due to changes of α are presented in Fig. 10(e) and 10(f).

It appears that you're engaged in a study or investigation focused on exploring diverse solution types (SSs) within a particular system or model, likely associated with wave behavior. Employing a method named SSEM (potentially representing Symbolic Simulation of Exact Models), your research aims to scrutinize the behavior of these solutions and their alterations contingent upon distinct values of a parameter denoted as FO, potentially indicating "Fractional Order" or a system-specific parameter. The graphical representations referenced in your explanation—such as 3-D plots, contour plots, and 2D graphs—essentially depict the obtained solutions for various FO values. These figures, labeled as Figs. 1 through 10, likely portray the visual manifestation of these SSs and their dynamic transformations, providing insights into their evolution in relation to fluctuations in the FO parameter. Utilizing visual representations, like graphs and plots, proves to be an effective method for visually articulating the behavior, characteristics, and alterations of solutions or patterns within the studied system. These graphical depictions serve to elucidate how these solutions change concerning shifts in the FO parameter, aiding both researchers and readers in comprehending the intricacies of the solutions' nature and their responses to parameter modifications. These visual aids act as essential tools, simplifying complex information and trends, thereby facilitating the interpretation and analysis of the acquired solutions within the framework of your research. They play a pivotal role in elucidating the interconnections, configurations, and transitions among various solution types under diverse conditions, thereby contributing significantly to a more profound comprehension of the system under scrutiny.
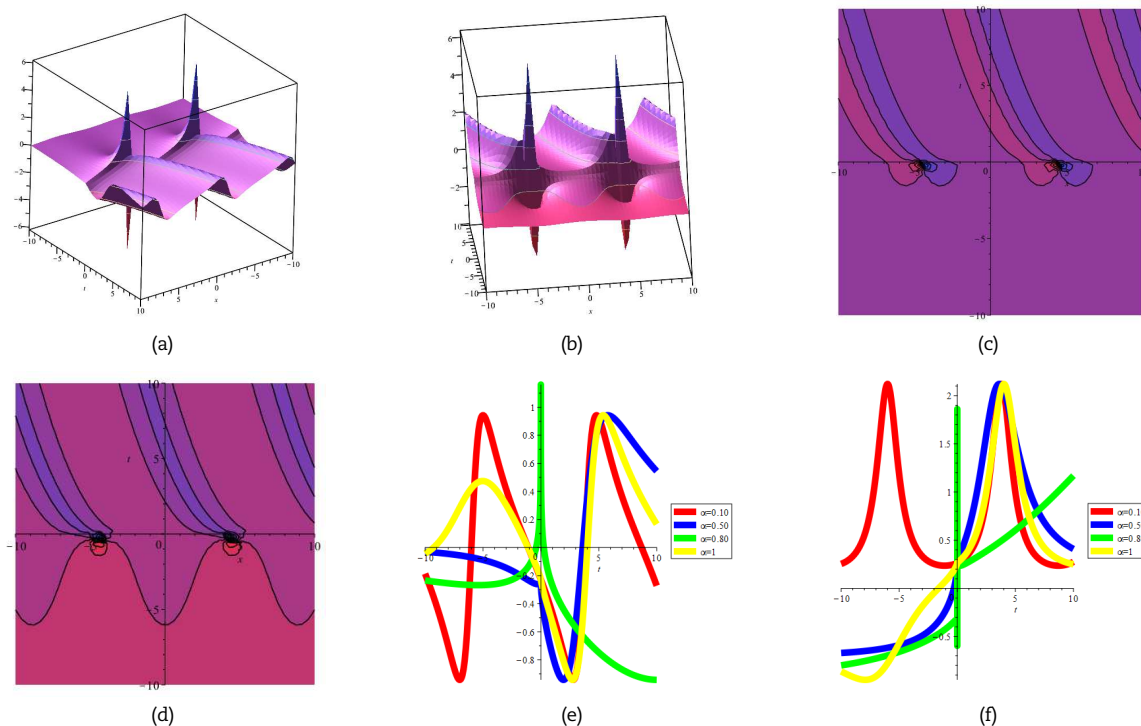

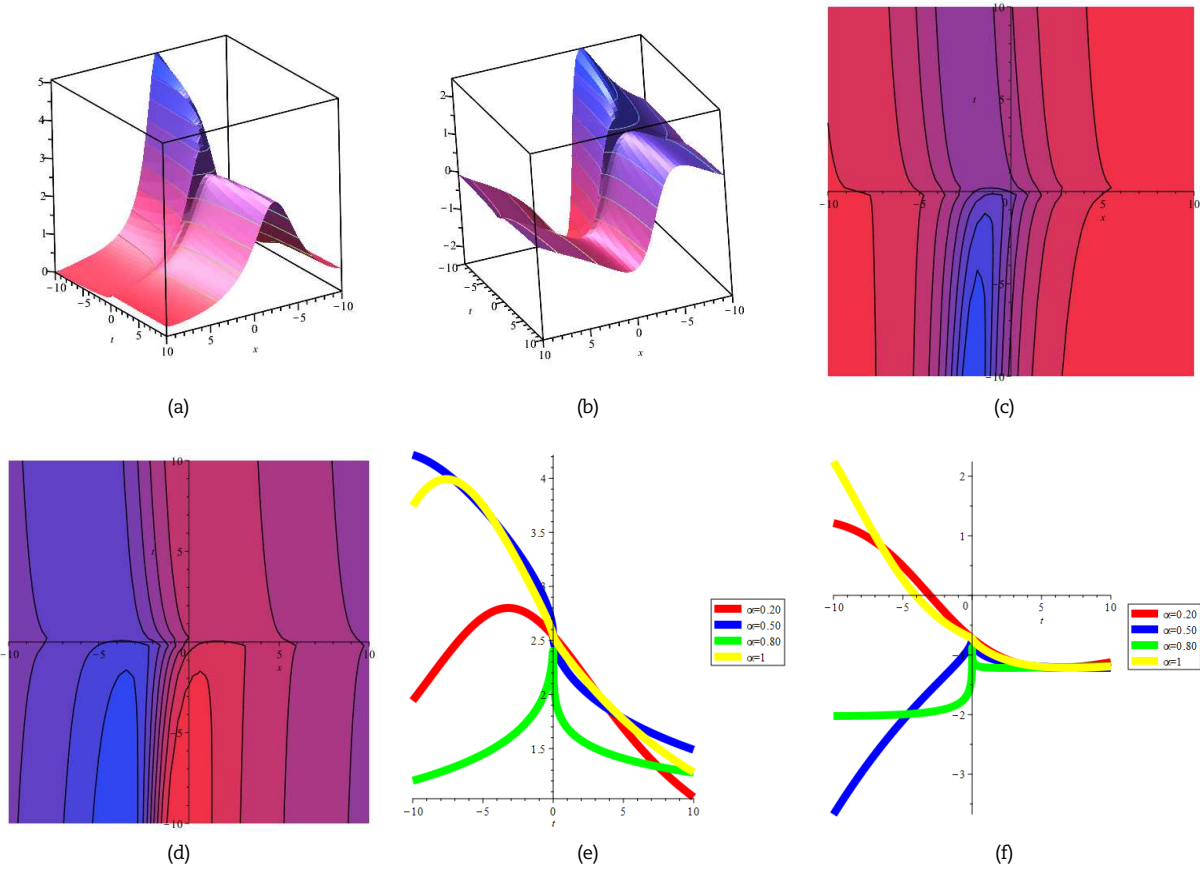| (a) | (b) | (c) |

| (d) | (e) | (f) |

Fig. 8. 3-D [(a) real and (b) complex], Contour [(c) real and (d) complex], and 2-D graph [(e) real and (f) complex] picture of $U_{19}^{\pm}(\eta)$ for $\alpha = 0.50$, $\beta = 0.25$, $\mu = 1$, $\lambda = 2$, $\eta_1 = 1$, $\eta_2 = 1$.
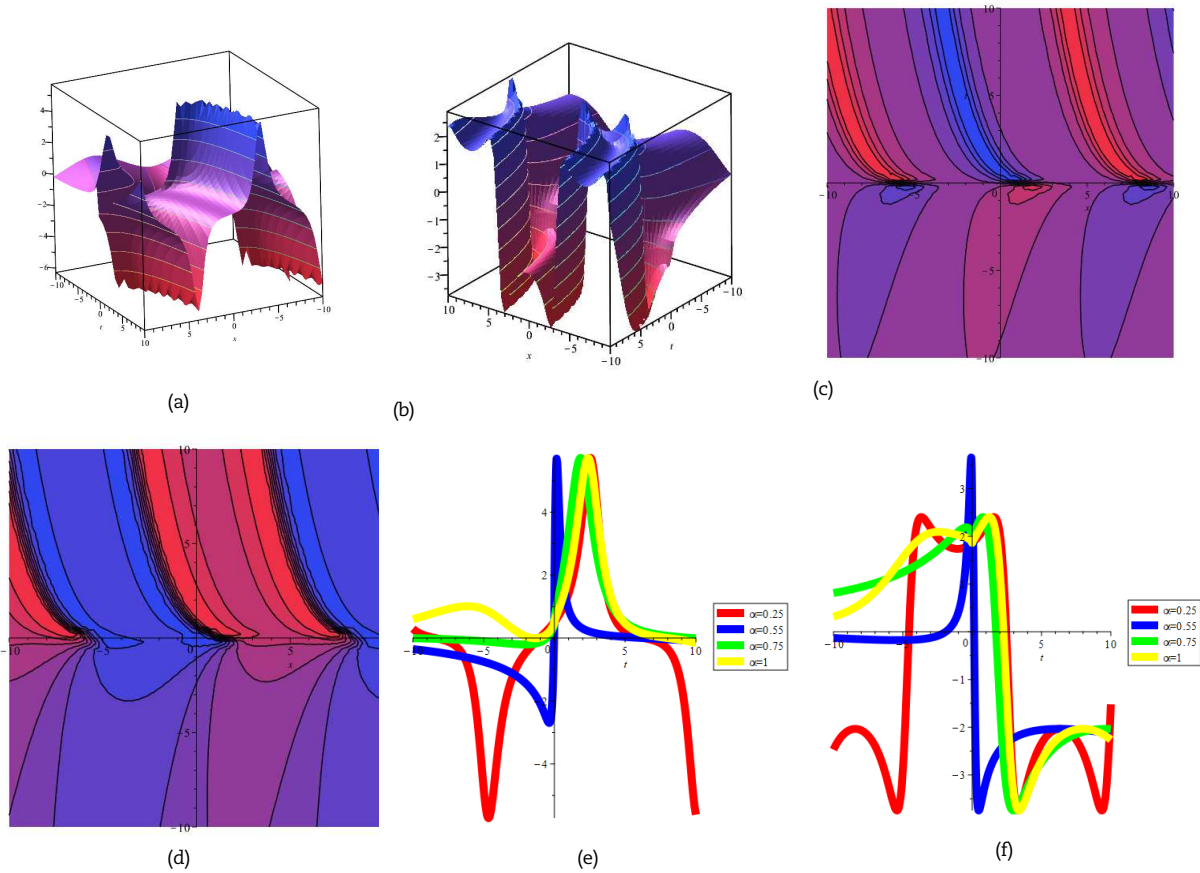
Fig. 9. 3-D [(a) real and (b) complex], Contour [(c) real and (d) complex], and 2-D graph [(e) real and (f) complex] picture of $U_{23}^{\pm}(\eta)$ for $\alpha = 0.50$, $\beta = 0.25$, $\mu = 1$, $\lambda = 2$, $\eta_1 = 1$, $\eta_2 = 1$.

Fig. 10. 3-D [(a) real and (b) complex], Contour [(c) real and (d) complex], and 2-D graph [(e) real and (f) complex] picture of $U_{26}^{\pm}(\eta)$ for $\alpha = 0.25$, $\beta = 0.10$, $\mu = 1$, $\lambda = 2$, $\eta_1 = 1$, $\eta_2 = 1$.

5. Conclusion

FMs, for example, the ferrites have been utilized in the energy and electronic industries. Overall, this paper contributed to our sympathetic of the K-M-M-S-MTD in the with/without of a DE which is employed in FMs and provides a valuable scheme for supervising NLFDEs. This paper designated the fruitful application of the SSEM to get new SSs for the K-M-M-S-M-T-D in the with/without of a DE. The obtained SSs were valuable for future experiments of the K-M-M-S-M-T-D and delivered insights into the performance of optical fiber communication, signal transmission, porous medium, magneto-acoustic waves in plasma, electromagnetism, fluid dynamics, chaotic systems, coastal engineering and so on. Since the K-M-M-S-M-T-D is so essential for expressing MFP in a FM-ZC, the got SSs are vital in realizing a wide-ranging diversity of charming and problematic nonlinear phenomena. The SSEM was shown to be a fruitful scheme for supervising NLFDEs. The SSs were designated graphically via 3D, contour and 2D for different values of FO through Maple software. We can study the K-M-M-S-M-T-D with a stochastic term in future work.

Author Contributions

All authors contributed equally and significantly to this paper. All authors have read and approved the final version of the manuscript.

Acknowledgments

Conflict of Interest

The authors declared that they have no known competing financial interests or personal relationships that could have appeared to influence the work reported in this paper.

Funding

Data Availability Statements

No datasets are associated with this manuscript. The datasets used for generating the plots and results during the current study can be directly obtained from the numerical simulation of the related mathematical equations in the manuscript.

Nomenclature

K-M-M-S-M-T-D	Kraenkel-Manna-Merle system with an M-truncated derivative
M-F-P	Magnetic field propagation
F-M-Z-C	Ferromagnetic materials with zero conductivity
S-S-E-M	Sardar sub-equation method
SSs	Soliton solutions
DE	Damping effect
3-D	Three-dimensional
2-D	Two-dimensional
FO	Fractional order
N-L-F-D-Es	Nonlinear fractional differential equations
FM	Ferromagnetic material
NLSE	Nonlinear science and engineering
FPs	Ferromagnetic particles

References

[1] Iqbal, N., Wu, R., Mohammed, W.W., Pattern formation induced by fractional cross-diffusion in a 3-species food chain model with harvesting, *Mathematics and Computers in Simulation*, 188, 2021, 102-119.
[2] Islam, S., Alam, M.N., Asad, M.F.A., Tunc, C., An analytical technique for solving new computational solutions of the modified Zakharov-Kuznetsov equation arising in electrical engineering, *Journal of Applied and Computational Mechanics*, 7(2), 2021, 715-726.
[3] Alam, M.N., Osman, M.S., New structures for closed-form wave solutions for the dynamical equations model related to the ion sound and Langmuir waves, *Communications in Theoretical Physics*, 73(3), 2021, 035001.
[4] Alam, M.N., Li, X., New soliton solutions to the nonlinear complex fractional Schrödinger equation and the conformable time-fractional Klein–Gordon equation with quadratic and cubic nonlinearity, *Physica Scripta*, 95, 2020, 045224.
[5] Dietl, T., Sato, K., Fukushima, T., Bonanni, A., Jamet, M., Barski, A., Kuroda, S., Tanaka, M., Hai, P.N., Yoshida, H.K., Spinodal nanodecomposition in semiconductors doped with transition metals, *Reviews of Modern Physics*, 87, 2015, 1311-1377.
[6] Shen, B.G., Sun, J.R., Hu, F.X., Zhang, H.W., Cheng, Z.H., Recent progress in exploring magnetocaloric materials, *Advanced Materials*, 21, 2009, 4545–4564.
[7] Tanaka, M., Ohya, S., Hai, P.N., Recent progress in III–V based ferromagnetic semiconductors: Band structure, Fermi level, and tunneling transport, *Applied Physics Reviews*, 1, 2014, 011102.
[8] Das, N., Ray, S.S., Exact traveling wave solutions and soliton solutions of conformable M-fractional modified nonlinear Schrödinger model, *Optik*, 287, 2023, 171060.
[9] Alsharidi, A.K., Bekir, A., Discovery of new exact wave solutions to the M-fractional complex three coupled Maccari's system by Sardar sub-equation scheme, *Symmetry*, 15, 2023, 1567.
[10] Faisal, K., Abbagari, S., Pashrashid, A., Houwe, A., Yao, S.W., Ahmad, H., Pure-cubic optical solitons to the Schrödinger equation with three forms of nonlinearities by Sardar subequation method, *Results in Physics*, 48, 2023; 106412.
[11] Asghari, Y., Eslami, M., Rezazadeh, H., Exact solutions to the conformable time-fractional discretized mKdv lattice system using the fractional transformation method, *Optical and Quantum Electron*, 55, 2023, 318.

[12] Hong, B., Exact solutions for the conformable fractional coupled nonlinear Schrödinger equations with variable coefficients, *Journal of Low Frequency Noise, Vibration & Active Control*, 42(2), 2023, 628-641.

[13] Yin, Q., Gao, B., Shi, Z., Distinct exact solutions for the conformable fractional derivative Gerdjikov-Ivanov equation via three credible methods, *Journal of Taibah University for Science*, 17, 2023, 2251219.

[14] Ahmad, H., Alam, M.N., Rahman, M.A., Alotaibid, M.F., Omri, M., The unified technique for the nonlinear time-fractional model with the beta-derivative, *Results in Physics*, 29, 2021, 104785.

[15] Ullah, M.S., Roshid, H.O., Ali, M.Z., New wave behaviors of the Fokas-Lenells model using three integration techniques, *PloS One*, 18(9), 2023, e0291071.

[16] Ullah, M.S., Mostafa, M., Ali, M.Z., Roshid, H.O., Akter, M., Soliton solutions for the Zoomeron model applying three analytical techniques, *PloS One*, 18(7), 2023, e0283594.

[17] Alam, M.N., Islam, S.M.R., The agreement between novel exact and numerical solutions of nonlinear models, *Partial Differential Equations in Applied Mathematics*, 8, 2023, 100584.

[18] Alam, M.N., An analytical technique to obtain traveling wave solutions to nonlinear models of fractional order, *Partial Differential Equations in Applied Mathematics*, 8, 2023, 100533.

[19] Alam, M.N., Soliton solutions to the electric signals in telegraph lines on the basis of the tunnel diode, *Partial Differential Equations in Applied Mathematics*, 7, 2023, 100491.

[20] Alam, M. N., Talib, I., Tunc, C., The new soliton configurations of the 3D fractional model in arising shallow water waves, *International Journal of Applied and Computational Mathematics*, 9, 2023, 75.

[21] Alam, M.N., Akash, H.S., Saha, U., Hasan, M.S., Parvin, M.W., Tunç, C., Bifurcation Analysis and Solitary Wave Analysis of the Nonlinear Fractional Soliton Neuron Model, *Iranian Journal of Science*, 2023, DOI: https://doi.org/10.1007/s40995-023-01555-y.

[22] Alam, M.N., Exact solutions to the foam drainage equation by using the new generalized (G'/G)-expansion method, *Results in Physics*, 5, 2015, 168-177.

[23] Alam, M.N., İlhan, O.A., Uddin, M.S., Rahim, M.A., Regarding on the results for the Fractional Clannish Random Walker's Parabolic equation and the nonlinear fractional Cahn-Allen equation, *Advances in Mathematical Physics*, 2022, 2022, 5635514.

[24] Nguepjouo, F.T., Kuetche, V.K., Kofane, T.C., Soliton interactions between multivalued localized waveguide channels within ferrites, *Physical Review E*, 89, 2014, 063201.

[25] Alshammari, M., Hamza, A.E., Cesarano, C., Aly, E.S., Mohammed, W.W., The Analytical Solutions to the Fractional Kraenkel–Manna–Merle System in Ferromagnetic Materials, *Fractal and Fractional*, 7, 2023, 523.

[26] Li, B.Q., Ma, Y.L., Rich soliton structures for the Kraenkel-Manna-Merle (KMM) System in Ferromagnetic Materials, *Journal of Superconductivity and Novel Magnetism*, 31, 2018, 1773–1778.

[27] Li, B.Q., Ma, Y.L., Oscillation rogue waves for the Kraenkel–Manna–Merle system in ferrites, *Journal of Magnetism and Magnetic Materials*, 537, 2021, 168182.

[28] Tripathy, A., Sahoo, S., Rezazadeh, H., Izgi, Z.P., Osman, M.S., Dynamics of damped and undamped wave natures in ferromagnetic materials, *Optik*, 281, 2023, 170817.

[29] Raza, N., Hassan, Z., Butt, A.R., Rahman, R.U., Aty, A.H.A., Mahmoud, M., New and more dual-mode solitary wave solutions for the Kraenkel–Manna–Merle system incorporating fractal effects, *Mathematical Methods in the Applied Sciences*, 45, 2022, 2964-2983.

[30] Zhang, L., Shen, B., Jiao, H., Wang, G., Wang, Z., Exact solutions for the KMM system in (2+1)-dimensions and its fractional form with beta-derivative, *Fractal and Fractional*, 6, 2022, 520.

[31] Jin, X.W., Lin, J., The contributions of Gilbert-damping and inhomogeneous exchange effects on the electromagnetic short waves propagation in saturated ferrite films, *Journal of Magnetism and Magnetic Materials*, 514, 2020, 167192.

[32] Ma, Y.L., Li, B.Q., Kraenkel-Manna-Merle saturated ferromagnetic system: Darboux transformation and loop-like soliton excitations, *Chaos, Solitons and Fractals*, 159, 2022, 112179.

[33] Tchokouansi, H.T., Felenou, E.T., Kuetche, V.K., Tchidjo, R.T., Dynamics of damped single valued magnetic wave in inhomogeneous circularly polarized ferrites, *Chinese Journal of Physics*, 78, 2022, 511-520.

[34] Shen, S.J., Li, H.J., Lin, J., Propagations of multiple solitons in a deformed ferrite, *Results in Physics*, 51, 2023, 106645.

[35] Jin, X.W., Lin, J., Rogue wave, interaction solutions to the KMM system, *Journal of Magnetism and Magnetic Materials*, 502, 2020, 166590.

[36] Li, B.Q., Ma, Y.L., Sathishkumar, P., The oscillating solitons for a coupled nonlinear system in nanoscale saturated ferromagnetic materials, *Journal of Magnetism and Magnetic Materials*, 474, 2019, 661-665.

[37] Mohammed, W.W., El-Morshedy, M., Cesarano, C., Al-Askar, F.M., Soliton Solutions of Fractional Stochastic Kraenkel–Manna– Merle Equations in Ferromagnetic Materials, *Fractal and Fractional*, 7, 2023, 328.

[38] Li, B.Q., Ma, Y.L., Loop-like periodic waves and solitons to the Kraenkel–Manna–Merle system in ferrites, *Journal of Electromagnetic Waves and Applications*, 32, 2018, 1275–1286.

[39] Sousa, J.V., Oliveira, E.C.D., A new truncated M-fractional derivative type unifying some fractional derivative types with classical properties, *International Journal of Analysis and Applications*, 16, 2018, 8396.

ORCID iD

Md. Nur Alam https://orcid.org/0000-0001-6815-678X
Md. Abdur Rahim https://orcid.org/0000-0003-2300-1420
Md. Najmul Hossain https://orcid.org/0000-0002-2528-9168
Cemil Tunç https://orcid.org/0000-0003-2909-8753

Publisher's Note Shahid Chamran University of Ahvaz remains neutral with regard to jurisdictional claims in published maps and institutional affiliations.